ADVANCED FUNCTIONAL MATERIALS
www.afm-journal.de

Materials Views
www.MaterialsViews.com

Assembly of Layered Rare-Earth Hydroxide Nanosheets and SiO_2 Nanoparticles to Fabricate Multifunctional Transparent Films Capable of Combinatorial Color Generation

*Byung-Il Lee, Eun-su Lee, and Song-Ho Byeon**

Colloidal solutions of layered rare-earth hydroxide nanosheets provide a simple route to deposit ultra thin luminescence films. The antireflection and antifogging properties were integrated into transparent luminescent films by the layer-by-layer assembly of Eu^{3+}, Tb^{3+}, Dy^{3+} doped-hydroxocation nanosheets and negatively-charged SiO_2 nanoparticles. Resulting multifunctional films exhibited efficient red, green, and blue emissions with controllable intensity. Highly improved transmittance enabled us to display combinatorial color luminescence, which can be achieved by multiply overlapping individual films with different combinations, without significant loss of transparency. Triple overlap of red/green/blue films generated an excellent white-light under 254 nm UV irradiation.

1. Introduction

Nanosheets of layered compounds are considered to be attractive building blocks for (ultra) thin films of controlled orientation.[1] The layer-by-layer (LbL) assembly method is frequently used to build functional multilayers of charged nanosheets with high transparency.[2] This technique is particularly suited for film deposition on non-flat surfaces with large areas. In the family of layered materials, layered rare-earth hydroxides (LRHs), $Re_2(OH)_5X \cdot mH_2O$ where Re = rare-earths and X = interlayer anions,[3] have received attention for potential application in luminescence films. Semitransparent films of oriented Gd_2O_3:Eu platelet crystallites were fabricated from the layered gadolinium hydroxide precursor film.[4] Multilayer films based on layered europium hydroxide and $Ti_{1.84}O_4$ nanosheets showed strong red emission attributed to the antenna effect of titanium oxide sheets.[5] In our previous work, highly transparent and highly luminescent Gd_2O_3:Eu films were prepared by allowing the formamide suspension containing exfoliated layered hydroxide nanosheets to dry on the substrate.[6] Annealing multilayers prepared by LbL deposition of Eu^{3+} and Tb^{3+} doped-layered gadolinium hydroxide and polystyrene sulfonate (PSS) led to a semitransparent film with multicolor emission capacity and color tunability.[7]

Antireflection (AR) surfaces are of great interest in many applications from military applications to coated displays and windows.[8] The reflection at the interface of the film can be completely suppressed when $n_f = (n_s n_0)^{1/2}$ (n_f, n_s, and n_0 are the refractive indices of the film, substrate, and transmitted medium, respectively.).[9] However, due to a lack of materials with sufficiently low refractive index, such an AR coating has commonly employed the assembly of multilayer thin films composed of oppositely charged nanoparticles.[10] Silica nanoparticles are often used to induce negatively-charged layers and high porosity in the assembled films.[11] A porous network created during the assembly process can achieve a refractive index low enough to produce broad-band AR surfaces that cover the visible light region.[12] Surface porosity and roughness are also closely related to the wettability of solid surfaces. For instance, thin films of (SiO_2/TiO_2) nanoparticle multilayers showed nanoporosity-driven superhydrophilic properties.[10a,13] This property, realized by the capillary effect on hydrophilic surfaces, has been investigated for self-cleaning, antifogging, and biocompatible applications.

When these AR surfaces are produced from inorganic materials, they exhibit high heat resistance, high chemical durability, and high weathering resistance. If we can integrate AR and antifogging properties into inorganic luminescent films with high transparency, these multifunctional films would have great potential for practical applications such as transparent wall and window displays. In the present work, we have explored an alternate assembly of activator doped-LRH hydroxocation nanosheets and negatively-charged SiO_2 nanoparticles on quartz glass substrates via LbL deposition to fabricate porous films. The resulting antireflective and antifogging films exhibited efficient red, green, and blue emissions with controllable intensity. Simple overlap of these multifunctional films generated combinatorial colors and bright white-light under commercial 254 nm UV irradiation, depending on the combination of individual films. Because of highly increased

B.-I. Lee,[†] E.-s. Lee,[†] Prof. S.-H. Byeon
Department of Applied Chemistry
College of Applied Science
Kyung Hee University
Gyeonggi 446-701, Korea
E-mail: shbyun@khu.ac.kr
[†] These authors equally contributed to this work.

DOI: 10.1002/adfm.201200295

transmittance, multiple overlap of films was not accompanied with any significant loss of transparency.

2. Results and Discussion

2.1. Assembly Behaviors of LGdH:Re Hydroxide Nanosheets and SiO_2 Nanoparticles

Simple, cheap, and large scale deposition on the substrate surface is desired for widely applicable thin films. Gadolinium oxide (Gd_2O_3) is known to be a good host for the luminescence of rare-earth ions.[14] Eu^{3+}, Tb^{3+}, and Dy^{3+} ions are generally used as efficient red, green, and blue luminescence centers in display applications, respectively.[15] To integrate the AR property into the luminescent films, it is needed to fabricate ultra thin films with high porosity. In this context, a simple precipitation method similar to previously reported procedures[16] was adopted in this work to prepare aqueous colloidal solutions containing nanosheets of activator doped-layered gadolinium hydroxides, $[Gd_{2.00-x}Re_x(OH)_5 \cdot mH_2O]^+Cl^-$ (LGdH:Re) where Re = Eu, Tb, and Dy. This method was effective for preparing a large amount of nanosheet colloidal suspension, where the majority of sheets are composed of double to triple hydroxide layers in the range of 2–3 nm in thickness. The concentration of activator was fixed to 10% (x = 0.20) for LGdH:Eu and LGdH:Tb and 5% (x = 0.10) for LGdH:Dy. **Figure 1**A shows X-ray diffraction (XRD) patterns of LGdH:Re hydroxide powder samples, which were collected by centrifugation of corresponding colloidal solutions. All the diffraction peaks are indexed as a layered gadolinium hydroxide structure reported in a previous study.[17] As observed in scanning electron microscopy (SEM) images in **Figure 2**A, all LGdH:Re powders consist of well developed sheets whose lateral dimensions are 150–200 nm.

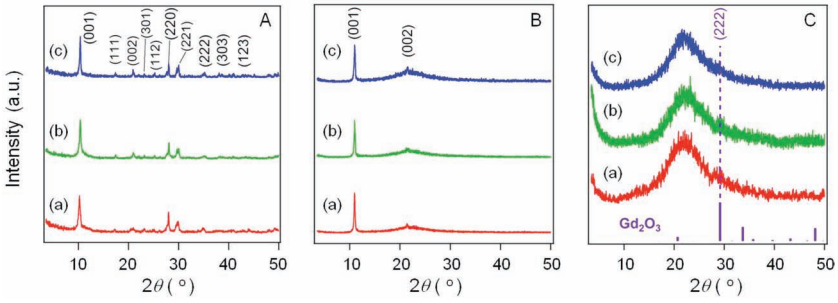

Figure 1. XRD patterns of (A) LGdH:Re powder and (LGdH:Re hydroxide nanosheet/SiO_2 nanoparticle)$_n$ films deposited on quartz glass slides (B) before and (C) after annealing at 600 °C. n = 7, 8, and 9 for Re = (a) Eu, (b) Tb, and (c) Dy. Diffractions for Gd_2O_3 refer to JCPDS Card No. 86-2477.

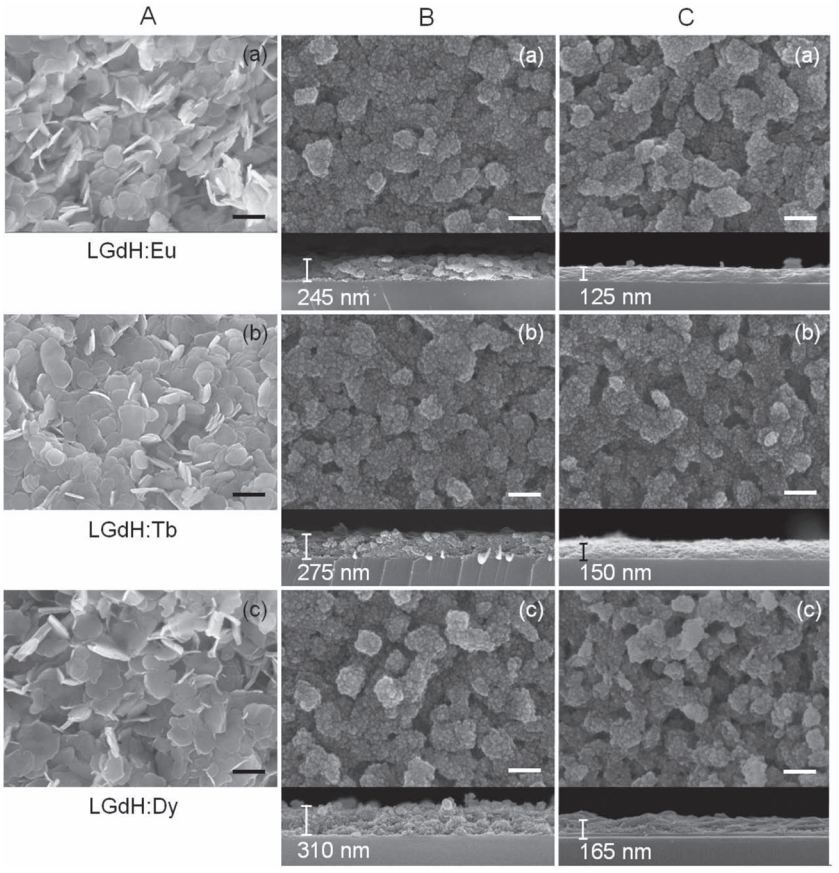

Figure 2. FE-SEM images of (A) LGdH:Re powder and (LGdH:Re hydroxide nanosheet/SiO_2 nanoparticle)$_n$ films deposited on quartz glass slides (B) before and (C) after annealing at 600 °C. n = 7, 8, and 9 for Re = (a) Eu, (b) Tb, and (c) Dy, respectively. Both surface (upper) and cross-sectional (lower) views are displayed for the films. Scale bars for powder and surface images = 200 nm.

Scheme 1 illustrates the LbL assembly process of LGdH:Re hydroxocation nanosheets and negatively-charged silica nanoparticles to fabricate porous films. Alternate dipping of quartz glass substrates (2 cm × 2 cm and 2 cm × 10 cm) in prepared aqueous colloidal solutions and SiO_2 (average size 10 ~ 15 nm) isopropyl alcohol solution produced highly transparent (LGdH:Re hydroxide nanosheet/SiO_2 nanoparticle)$_n$ films. The thickness of the films was controlled by the number of deposition cycles (n). Roughly, six to ten deposition cycles (n = 6–10) of hydroxide nanosheets and SiO_2 nanoparticles resulted in transparent films of 200–350 nm in thickness. As an example for the optimized color overlap of different brightness films, particularly for the efficient white-light generation, the number of deposition cycles for tri-color films in this paper was selected as 7, 8, and 9 for Re = Eu (red), Tb (green), and Dy (blue) films, respectively.

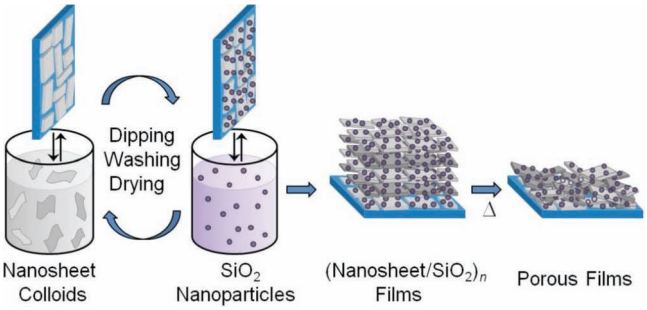

Scheme 1. Alternate depositions of LGdH:Re (Re = Eu, Tb, and Dy) hydroxocation nanosheets and negatively-charged SiO_2 nanoparticles on a quartz glass substrate for the fabrication of multifunctional porous films.

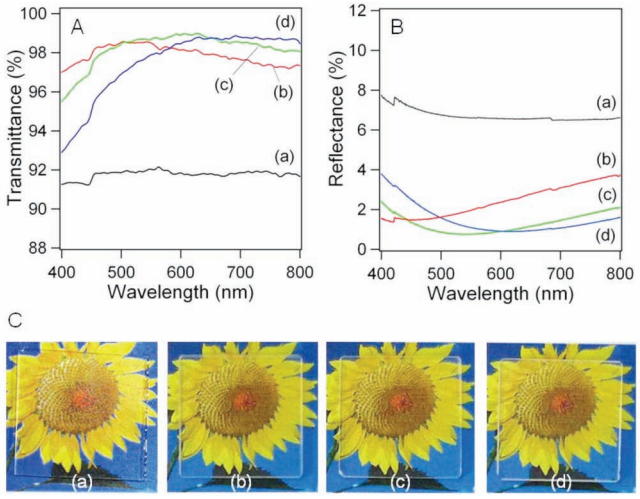

Figure 3. (A) Transmittance and (B) reflectance spectra and (C) photographs in day light of (Gd_2O_3:Re nanosheet/SiO_2 nanoparticle) films obtained after annealing (LGdH:Re hydroxide nanosheet/SiO_2 nanoparticle)$_n$ films at 600 °C. (a) bare quartz glass and n = 7, 8, and 9 for Re = (b) Eu, (c) Tb, and (d) Dy, respectively.

XRD patterns of (LGdH:Re hydroxide nanosheet/SiO_2 nanoparticle)$_n$ films are shown in Figure 1B. Compared with those of the powder samples, the absence of (*hkl*) diffraction peaks except sharp (00*l*) ones in XRD patterns of corresponding films suggests the preferential orientation of hydroxide nanosheets parallel to the substrate surface. Figure 2B shows the surface and cross sectional SEM images of (LGdH:Re hydroxide nanosheet/SiO_2 nanoparticle)$_n$ films. Consistently with XRD patterns, hydroxide nanosheets assembled on the substrate are oriented parallel to the surface and covered with SiO_2 nanoparticles. Films of 245, 275, and 310 nm in average thickness were fabricated by 7, 8, and 9 cycle depositions of hydroxide nanosheets and SiO_2 nanoparticles, respectively.

2.2. Antireflection and Antifogging Properties of (Gd_2O_3:Re Nanosheet/SiO_2 Nanoparticle) Films

When annealing (LGdH:Re hydroxide nanosheet/SiO_2 nanoparticle)$_n$ films at 600 °C, the (00*l*) diffraction peaks originating from layered hydroxide phases disappeared and weak (222) diffraction of Gd_2O_3 appeared as exhibited in Figure 1C. The similarity between (001) plane of LGdH hydroxide and (222) plane of Gd_2O_3 can induce a quasitopotactic transformation from the hydroxide film to the oxide film with the preferential [111] orientation parallel to the substrate surface.[4] Although LGdH hydroxide was partially transformed to GdOCl in two-dimensionally confined thick films,[7] similar transformation was not observed in ultra thin LGdH hydroxide films in this work. When we measured XRD patterns of bulk powder precipitated from the mixture of LGdH:Eu colloidal solution and SiO_2 solution, an amorphous phase was obtained after heating above 600 °C for the same duration and partially crystallized to Gd_2SiO_5 at 1000 °C (see Supporting Information, Figure S1). Thus, annealing the films at temperatures higher than 600 °C initiated the reaction of Gd_2O_3:Re and SiO_2 to reduce the surface porosity of films, and consequently resulted in significantly decreased transparency and the loss of antireflective and superhydrophilic properties. (Gd_2O_3:Re nanosheet/SiO_2 nanoparticle) films were accordingly obtained by annealing hydroxide films at 600 °C. Additional reduction process was required for (Gd_2O_3:Tb nanosheet/SiO_2 nanoparticle) films (see Experimental section). As observed in the surface SEM images of Figure 2C, Gd_2O_3:Re produced by annealing show a sheet-structure whose morphology and preferential orientation are not significantly different from those of the corresponding hydroxide nanosheets. In contrast, as measured in cross sectional images, the average thickness of the final (Gd_2O_3:Re nanosheet/SiO_2 nanoparticle) films was reduced to 120–170 nm. For antireflection applications, the film should have a thickness of a quarter of the visible wavelength (ca. 100–170 nm) to enhance destructive interference of the reflected light.[9] As nanopores in (TiO_2/SiO_2) nanoparticle multilayer films were retained after annealing at 550 °C,[10a] SiO_2 nanoparticles covering Gd_2O_3:Re nanosheets maintain high film porosity despite the considerable reduction in thickness by annealing.

The transmittance and reflectance of both (LGdH:Eu hydroxide nanosheet/SiO_2 nanoparticle)$_n$ and corresponding (Gd_2O_3:Eu nanosheet/SiO_2 nanoparticle) films were strongly improved with increasing the number of deposition cycles upto n = 10 (see Supporting Information, Figure S2). The wavelength of maximum suppression of reflections is determined by the quarter-wave optical thickness of the coatings and consequently shifts to the longer wavelength region with increasing film thickness.[9] **Figure 3** compares the transmittance and reflectance curves of Re = Eu (n = 7), Tb (n = 8), and Dy (n = 9) films after annealing with those of the bare quartz substrate in the visible wavelength region. Despite as-prepared (LGdH:Re hydroxide nanosheet/SiO_2 nanoparticle)$_n$ films exhibited sufficiently high transparency comparable to that of the bare quartz substrate (Supporting Information, Figure S3), porous (Gd_2O_3:Re nanosheet/SiO_2 nanoparticle) films obtained after annealing showed more improved transparency. The quartz glasses coated with (Gd_2O_3:Eu nanosheet/SiO_2

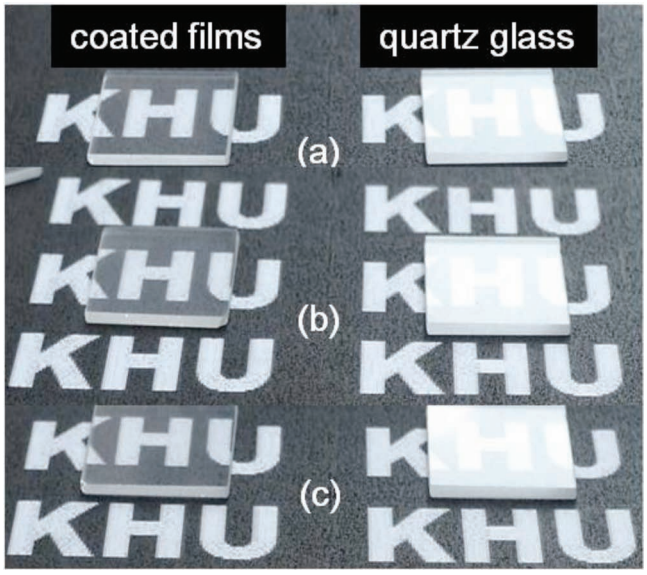

Figure 4. Photographs of (Gd_2O_3:Re nanosheet/SiO_2 nanoparticle) films deposited on quartz glass slides and bare quartz glasses under sun light, showing the suppression of reflection. Re = (a) Eu (n = 7), (b) Tb (n = 8), and (c) Dy (n = 9).

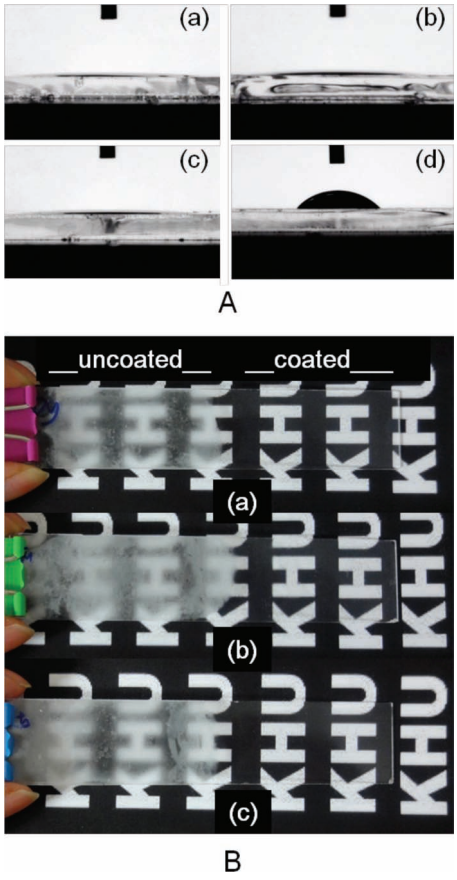

Figure 5. (A) Shapes of water droplet on (Gd_2O_3:Re nanosheet/SiO_2 nanoparticle) films, Re = (a) Eu (n = 7), (b) Tb (n = 8), (c) Dy (n = 9), and (d) bare quartz glass (water contact angle ~35°). (B) Photographs of (Gd_2O_3:Re nanosheet/SiO_2 nanoparticle)-coated (right portion) and uncoated quartz glass slide (left portion) after being cooled below −5 °C for 3 h in a refrigerator followed by exposure to humid laboratory air (higher than 50% in relative humidity). Re = (a) Eu, (b) Tb, and (c) Dy.

nanoparticle) and (Gd_2O_3:Tb nanosheet/SiO_2 nanoparticle) films (average thickness of around 120–150 nm) show 5–7% higher transmittance (96–99%) and 5–7% lower reflectance (1–3%) in comparison with those of the bare quartz glass over the visible wavelength range, confirming the improvement in antireflection effect. The maximum transmittance and minimum reflectance of (Gd_2O_3:Dy nanosheet/SiO_2 nanoparticle) film of 164 nm in average thickness is close to 99% and 1%, respectively, at wavelengths longer than 550 nm. As shown in Figure 3C, no difference in transparency between the coated and the bare quartz glasses is observed to the naked eye in day light. The excellent antireflection (AR) performance of (Gd_2O_3:Re nanosheet/SiO_2 nanoparticle) films is displayed in photographs of **Figure 4**, taken under sunlight. The legibility of the white text on a black background behind glass samples coated with (Gd_2O_3:Re nanosheet/SiO_2 nanoparticle) films is considerably better than that behind the bare quartz glasses whose reflectivity almost buries the text.

The wettability of the prepared films was characterized by the water droplet contact angle (WCA) and the speed of water spreading on the surface. As shown in **Figure 5**A, compared with that on the bare quartz glass (around 35°), WCAs on (Gd_2O_3:Re nanosheet/SiO_2 nanoparticle) films were less than 5° in less than 0.5 s after dropping on the surface. This superhydrophilicity generally leads to antifogging properties; the network of capillaries present in porous films provide good channels for fast spreading of a water droplet on the film. The antifogging effect of (Gd_2O_3:Re nanosheet/SiO_2 nanoparticle) films was demonstrated by exposing partly coated quartz glass slides to humid environments (higher than 50% in relative humidity) after cooling them at a low temperature (below −5 °C). The photographs in Figure 5B show that the bare portion of quartz glass immediately fogged to scatter light whereas the (Gd_2O_3:Re nanosheet/SiO_2 nanoparticle)-coated portion remained transparent, confirming the apparent antifogging effect.

2.3. Photoluminescence Properties of (Gd_2O_3:Re Nanosheet/SiO_2 Nanoparticle) Films

In contrast to the increasing tendancy of transmittance (upto n = 10), it was expected that the photoemission of multifunctional films be enhanced with the number of deposition cycles of LGdH:Re and SiO_2. In **Figure 6**, photographs of (Gd_2O_3:Eu nanosheet/SiO_2 nanoparticle) films in day light visually verify the optical transparency. Photographs of films under 254 nm UV irradiation demonstrate an increase of luminescent brightness as a function of deposition cycles (n) for the corresponding hydroxide films. The photoluminescence spectra of all n = 2, 4, 6, 8, and 10 films, measured at the excitation wavelength of 254 nm, showed typical $^5D_0 \rightarrow {}^7F_J$ transitions of Eu^{3+} ions. The enhancement behavior of emission intensity with increasing n

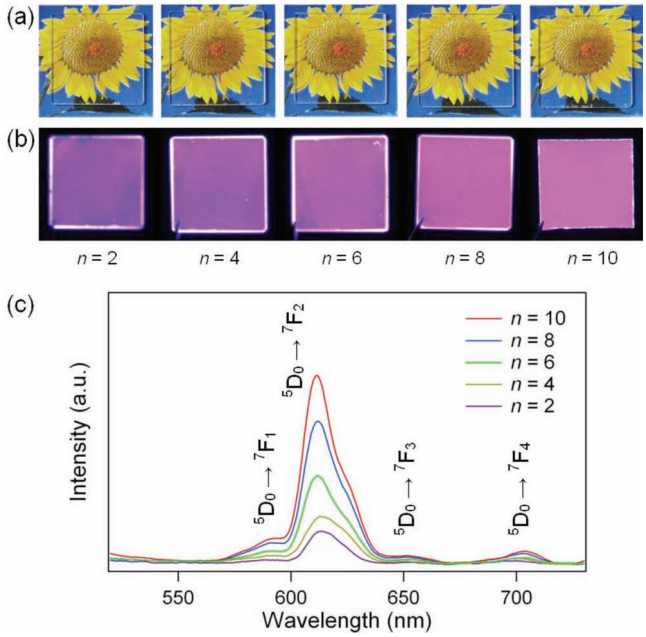

Figure 6. Photographs (a) in day light and (b) under 254 nm UV irradiation and (c) photoluminescence spectra (λ_{ex} = 254 nm) of (Gd_2O_3:Eu nanosheet/SiO_2 nanoparticle) films obtained after annealing (LGdH:Eu hydroxide nanosheet/SiO_2 nanoparticle)$_n$ films at 600 °C as a function of n.

is consistent with visual display of the same films. Because a deposition of (Gd_2O_3:Eu nanosheet/SiO_2 nanoparticle) layers thicker than n = 10 is accompanied by lower transmittance of film, the luminescence intensity and transparency should be optimized depending on the application. The photoemission of film was also enhanced by increasing the annealing temperature upto 600 °C. However, an annealing above 700 °C strongly reduced the emission intensity of films (Supporting Information, Figure S4).

Figure 7 shows the photoluminescence spectra and photographs of tri-color films obtained by annealing (LGdH:Re hydroxide nanosheet/SiO_2 nanoparticle)$_n$ films (n = 7, 8, and 9 for Re = Eu, Tb, and Dy, respectively). Irradiating with 254 nm UV, (Gd_2O_3:Re nanosheet/SiO_2 nanoparticle) coated-quartz glasses exhibit bright red, green, and blue emissions for Re = Eu, Tb, and Dy, respectively. Uniform luminescence illustrates the fabrication of a high-quality phosphor layer on the quartz substrate. The emission spectrum of (Gd_2O_3:Eu nanosheet/SiO_2 nanoparticle) film (Figure 7a), measured at an excitation wavelength of 254 nm, shows typical strong emission at 610 nm (red) and weak emission around 590 nm (orange), which are attributed to $^5D_0 \rightarrow {}^7F_2$ and $^5D_0 \rightarrow {}^7F_1$ transitions of $Eu^{3+}(4f^6)$ ions, respectively. (Gd_2O_3:Tb nanosheet/SiO_2 nanoparticle) film shows two emissions at 485 (blue) and 545 nm (green) ascribed to $^5D_4 \rightarrow {}^7F_6$ and $^5D_4 \rightarrow {}^7F_5$ transitions of $Tb^{3+}(4f^8)$ ions, respectively (Figure 7b).[18] The characteristic emission of $Dy^{3+}(4f^9)$ ions is dominated by relatively weak two main groups in the blue region (485 nm) and the yellow region (575 nm) corresponding to $^4F_{9/2} \rightarrow {}^6H_{15/2}$ and $^4F_{9/2} \rightarrow {}^6H_{13/2}$ transitions, respectively (Figure 7c).[19] An increase of the emission intensity at wavelength region shorter than ~ 470 nm was attributed to the quartz substrate under 254 nm UV irradiation (see Supporting Information, Figure S5 for the emission spectrum of bare quartz substrate). It is noted that these brightnesses are generated from ultra thin luminescent films of 96–99% transmittance (Figure 3). When we deposited a thicker (Gd_2O_3:Re nanosheet/SiO_2 nanoparticle) layer on the quartz glass (n = 20), no visual difference in transparency was observed between the bare quartz substrate and coated films as shown in **Figure 8**A. Compared with those of the AR films (n = 7 ~ 9), the transmittance of n = 20 films at around 550 nm is much lower but close to that (~92%) of the bare quartz glass (Figure 8B; see Supporting Information, Figure S6 for the corresponding reflectance spectra). In contrast, the photoluminescence intensity is significantly enhanced with increasing the number of deposition cycles, as expected (Figure 8C). However, despite high transparency comparable with the bare quartz glass, the fabrication of such a relatively thick film resulted in a loss of antireflection and antifogging properties.

2.4. Combinatorial Color and White-Light Generation by Overlapping Individual (Gd_2O_3:Re Nanosheet/SiO_2 Nanoparticle) Films with Different Combinations

Figure 9 compares the transmittance spectra and photographs of doubly and triply overlapped (Gd_2O_3:Re nanosheet/SiO_2 nanoparticle) films in daylight and under 254 nm UV irradiation, to visually verify the optical transparency and high luminescent brightness (see Supporting Information, Figure S7 for the corresponding reflectance spectra). The optical transmittances of overlapped films are higher than those of overlapped bare glasses in the visible wavelength region (Figure 9A). Because of the AR effect of individual Re = Eu, Tb, and Dy films (Figure 3), doubly and even triply overlapped films are sufficiently transparent and their transmittances are comparable with that (~92%) of single quartz glass so that the

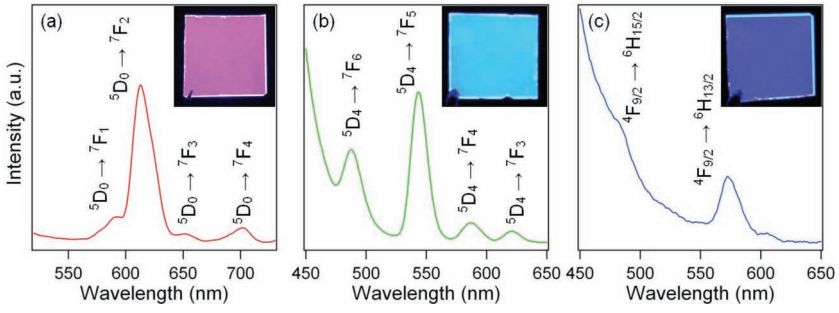

Figure 7. Photoluminescence spectra measured at 254 nm excitation of (Gd_2O_3:Re nanosheet/SiO_2 nanoparticle) films obtained after annealing (LGdH:Eu hydroxide nanosheet/SiO_2 nanoparticle)$_n$ films; n = 7, 8, and 9 for Re = (a) Eu, (b) Tb, and (c) Dy, respectively. (inset: photographs when irradiated with 254 nm UV).

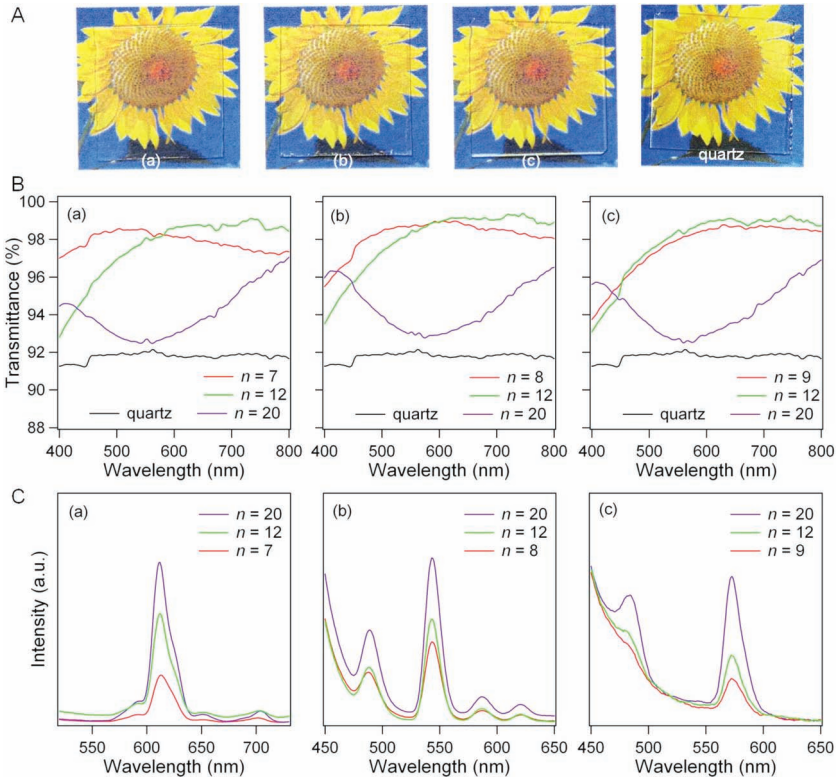

Figure 8. (A) Photographs of (Gd_2O_3:Re nanosheet/SiO_2 nanoparticle) films obtained after annealing (LGdH:Re hydroxide nanosheet/SiO_2 nanoparticle)$_n$ films of n = 20. Comparison of (B) transmittance and (C) photoluminescence spectra measured at 254 nm excitation of n = 7 ~ 20 films. Re = (a) Eu, (b) Tb, and (c) Dy.

flower behind them is clearly discernible to the naked eye in Figure 8B.

Combinatorial color luminescence is readily displayed by overlapping individual red (Re = Eu), green (Re = Tb), and blue (Re = Dy) films as shown in Figure 9C. Because the $^5D_4 \rightarrow {}^7F_6$ transition of Tb^{3+} (485 nm) overlaps the relatively weak $^4F_{9/2} \rightarrow {}^6H_{15/2}$ transition of Dy^{3+} to enhance the blue emission (Figure 9D), triple overlap of red/green/blue films generates an excellent white-light. This demonstrates the potential application of our films as a transparent white luminescent source. Moreover, no energy/charge transfer can occur between overlapped films. Considering that the charge transfer between different luminescent components decreases the color purity and stability in tunable multicolor light-emitting materials based on organic luminescent systems,[20] the color tuning by simple overlap of (Gd_2O_3:Re nanosheet/SiO_2 nanoparticle) films would be suitable for white-light emission. If we adjust the intensities of colors by controlling the number of deposition cycles, a system capable of finely tunable color generation could be developed, where different combinations of films can generate diverse colors. Because of different annealing conditions for red, green, and blue-emitting films, the simultaneous deposition of tricolor sources on a single substrate is practically difficult. The combinatorial color system that is realized by multiple overlap of individual antireflection color films with different combinations would have great potential for the transparent display including transparent white-light generation.

3. Conclusions

In conclusion, we successfully integrated AR and antifogging properties into the transparent luminescent films using LbL assembly of LGdH:Re hydroxocation nanosheets and SiO_2 nanoparticles. Annealed films have several advantages for multicolor displays. The control of film thickness (i.e. the number of deposition cycle) and combination of films can balance the differences in luminous efficiency and intensity between different color films to provide tunable combinatorial color luminescence. High transparency with AR and antifogging properties would meet the requirement for transparent optoelectronic applications. White-light emission with controllable color purity and stability can be achieved by simply overlapping tri-color films, where no charge transfer is possible between the different color components.

4. Experimental Section

Materials: $GdCl_3{\cdot}6H_2O$, $EuCl_3{\cdot}6H_2O$, $TbCl_3{\cdot}6H_2O$, and $DyCl_3{\cdot}6H_2O$ were obtained from Sigma-Aldrich. SiO_2 colloidal solution was obtained from Nissan Chemical. The diameter of SiO_2 particles was 10–15 nm according to Nissan Chemical. SiO_2 colloidal solution (30–31 wt%) was diluted and used for assembly. All reagents were used as purchased without any further purification.

Preparation of colloidal solutions of LGdH:Re (Re = Eu, Tb, and Dy): The aqueous suspensions of $Gd_{2.00-x}Re_x(OH)_5Cl{\cdot}mH_2O$ (Re = Eu, Tb, and Dy) were prepared according to the slightly modified procedure of previous report.[16] The concentration of activator was fixed to 10% (x = 0.20) for LGdH:Eu and LGdH:Tb and 5% (x = 0.10) for LGdH:Dy. Typically, stoichiometric amounts of $GdCl_3{\cdot}6H_2O$, $EuCl_3{\cdot}6H_2O$, $TbCl_3{\cdot}6H_2O$, and $DyCl_3{\cdot}6H_2O$ were dissolved in water to prepare aqueous solutions (5.0 mM, 100 mL). After a clear solution was formed by uniform stirring, aqueous KOH solution (10 mM, 100 mL) was added drop-wise at room temperature. The resulting colloidal mixture was heated at 60 °C for 12 h while stirring. After the reaction was completed, the colloidal suspensions were used to deposit the corresponding films. To measure the X-ray diffraction patterns and SEM images, the solid products were collected by centrifugation, washed with deionized water, and dried at 40 °C for a day. The dopant (Eu, Tb, and Dy) content and chemical compositions of the obtained products were confirmed using ICP and TG analyses (see Supporting Information, Table S1 and Figure S8, respectively). The experimental values were in agreement with the nominal compositions within experimental errors, i.e., $Gd_{1.80}Eu_{0.20}(OH)_5Cl{\cdot}1.5H_2O$ (LGdH:Eu), $Gd_{1.80}Tb_{0.20}(OH)_5Cl{\cdot}1.0H_2O$ (LGdH:Tb), and $Gd_{1.90}Dy_{0.10}(OH)_5Cl{\cdot}1.0H_2O$ (LGdH:Dy).

Fabrication of porous films by an alternate assembly of LGdH:Re nanosheets and SiO_2 nanoparticles (Re = Eu, Tb, and Dy): The quartz glass slides (2 cm × 2 cm and 2 cm × 10 cm) were placed in a concentrated H_2SO_4/H_2O_2 solution (7/3 by volume) for 30 min and washed with copious amounts of deionized water. Well dried quartz glass slides

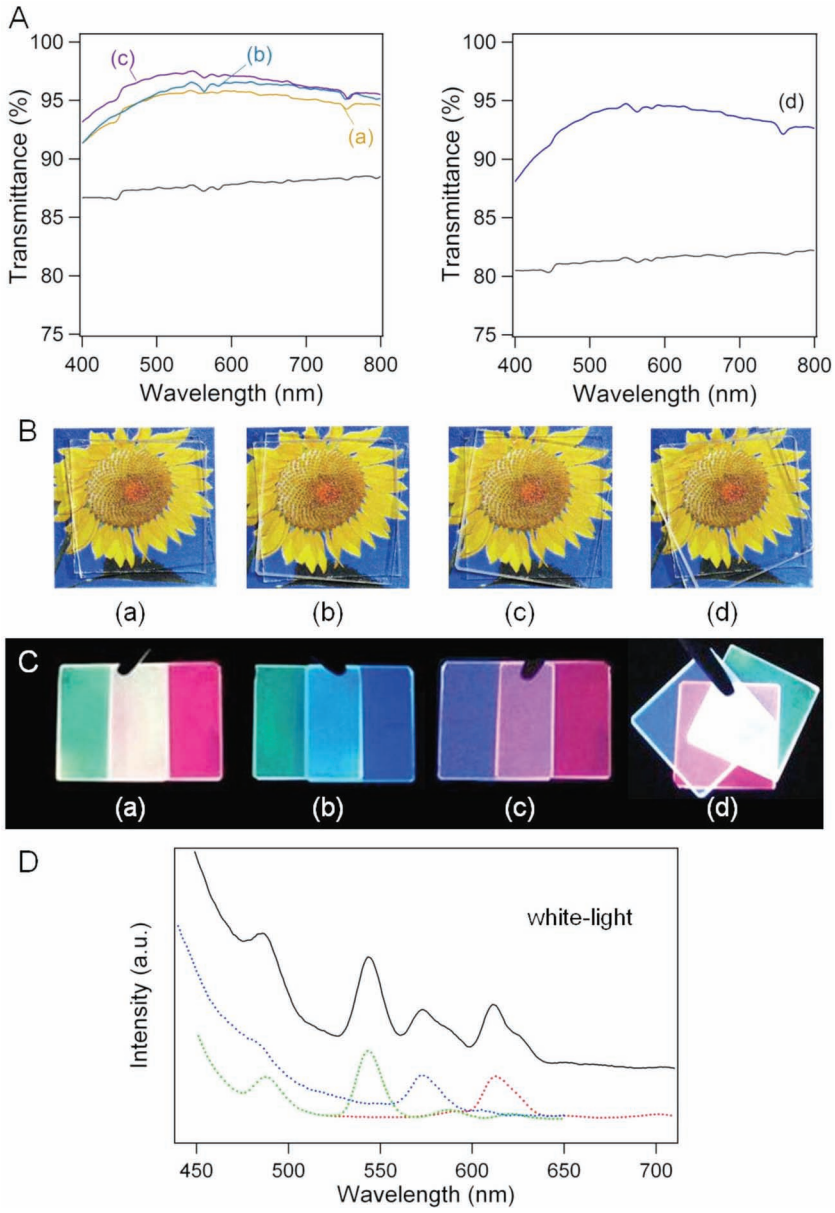

Figure 9. (A) Transmittance spectra and photographs of multiply overlapped (Gd_2O_3:Re nanosheet/SiO_2 nanoparticle) films deposited on quartz glass substrates (B) in day light and (C) under the 254 nm UV excitation. Re = (a) Tb/Eu, (b) Dy/Tb, (c) Dy/Eu, (d) Dy/Tb/Eu. (D) Photoluminescence spectra of triply overlaped film (solid line) and individual Re = Eu (red; $n = 7$), Tb (green; $n = 8$), and Dy (blue; $n = 9$) films (dotted lines). Black curves in (A) are transmittance spectra of doubly and triply overlapped bare quartz glasses.

were then immersed into colloidal solutions of corresponding activator doped-gadolinium hydroxocation (LGdH:Re) nanosheets for 12 h and rinsed with water. Nanosheets coated quartz slides were dipped into SiO_2/isopropyl alcohol (IPA) solution (0.1 wt%) for 30 s, followed by washing with water. This deposition cycle for LGdH:Re nanosheets and SiO_2 nanoparticles was repeated several times to produce (LGdH:Re nanosheet/SiO_2 nanoparticle)$_n$ multilayer films (n = 2–20). The immersion period in colloidal suspensions of LGdH:Re was adjusted to 20 min from the second deposition cycle. The number of deposition cycles (n) is variable for the color tuning of overlapped red, green, and blue films. In this work, red (Re = Eu), green (Re = Tb), and blue (Re = Dy) films particularly for the white-light generation were fabricated with n = 7, 8, and 9, respectively, depending on the brightness of the film. Porous (Gd_2O_3:Re nanosheet/SiO_2 nanoparticle) films were obtained by annealing these hydroxide films. The (LGdH:Re hydroxide nanosheet/SiO_2 nanoparticle)$_n$ films (Re = Eu and Dy) on a quartz substrate were annealed in air at 600 °C for 5 h and 12 h, respectively. The (LGdH:Tb hydroxide nanosheet/SiO_2 nanoparticle)$_n$ film was annealed in air at 600 °C for 2 h and then under a flow of mixed gas (Ar + 4% H_2) at 250 °C for 12 hr.

Characterizations: Powder X-ray diffraction patterns were recorded on a rotating anode installed diffractometer (MacScience Model M18XHF). The Cu Kα radiation used was monochromated by a curved-crystal graphite. Field emission scanning electron microscopy (FE-SEM) was carried out with a Carl Zeiss LEO SUPRA 55 electron microscope operating at 30 kV. Optical transmittance of films was measured with UV–vis spectrophotometers, Shimadzu Multispec-1501 and a LAMBDA 35. Water droplet contact angles (WCAs) of surfaces were measured using a Phoenix 150 Surface Electro Optics (SEO) at room temperature. Water droplets about 0.5 μL in volume were dropped carefully onto the sample surfaces. To examine the antifogging property of assembled films, a slide glass with both uncoated and Gd_2O_3:Re/SiO_2 coated portions was cooled below −5 °C for 3 h in a refrigerator, and then exposed to humid laboratory air (higher than 50% in relative humidity). The photoluminescence spectra were measured at room temperature using a FP-6600 spectrophotometer (JASCO) with a Xenon flash lamp.

Supporting Information

Supporting Information is available from the Wiley Online Library or from the author.

Acknowledgements

This work was supported by the Mid-career Researcher Program through National Research Foundation (NRF) grant funded by the Ministry of Education, Science and Technology (MEST) (No. 2011-0014763). Supporting Information is available online from Wiley InterScience or from the author.

Received: January 31, 2012
Revised: March 22, 2012
Published online: May 9, 2012

[1] a) C. Chen, P. Gunawan, X. W. Lou, R. Xu, *Adv. Funct. Mater.*, DOI: 10.1002/adfm.201102333; b) R. Ma, T. Sasaki, *Adv. Mater.* **2010**, *22*, 5082; c) T. Kameyama, K. Okazaki, K. Takagia, T. Torimoto, *Phys. Chem. Chem. Phys.* **2009**, *11*, 5369; d) J. B. Han, J. Lu, M. Wei, Z. L. Wang, X. Duan, *Chem. Commun.* **2008**, 5188; e) J. H. Lee, S. W. Rhee, D. Y. Jung, *J. Am. Chem. Soc.* **2007**, *129*, 3522.
[2] a) G. Singh, S. Pillai, A. Arpanaei, P. Kingshott, *Adv. Funct. Mater.* **2011**, *21*, 2556; b) J. Zhao, X. Kong, W. Shi, M. Shao, J. Han, M. Wei,

D. G. Evans, X. Duan, *J. Mater. Chem.* **2011**, *21*, 1392; c) K. K. Manga, Y. Zhou, Y. Yan, K. P. Loh, *Adv. Funct. Mater.* **2009**, *19*, 3638; d) D. Yan, J. Lu, M. Wei, J. Han, J. Ma, F. Li, D. G. Evans, X. Duan, *Angew. Chem. Int. Ed.* **2009**, *48*, 3073; e) Z. Liu, R. Ma, M. Osada, N. Iyi, Y. Ebina, K. Takada, T. Sasaki, *J. Am. Chem. Soc.* **2006**, *128*, 4872.

[3] a) Y. Xiang, X.-F. Yu, D.-F. He, Z. Sun, Z. Cao, Q.-Q. Wang, *Adv. Funct. Mater.* **2011**, *21*, 4388; b) F. Geng, R. Ma, T. Sasaki, *Acc. Chem. Res.* **2010**, *43*, 1177; c) K.-H. Lee, S.-H. Byeon, *Eur. J. Inorg. Chem.* **2009**, 929; d) L. Poudret, T. J. Prior, L. J. McIntyre, A. M. Fogg, *Chem. Mater.* **2008**, *20*, 7447; e) F. Gandara, J. Perles, N. Snejko, M. Iglesias, B. Gomez-Lor, E. Gutierrez-Puebla, M. A. Monge, *Angew. Chem., Int. Ed.* **2006**, *45*, 7998.

[4] L. Hu, R. Ma, T. C. Ozawa, T. Sasaki, *Angew. Chem. Int. Ed.* **2009**, *48*, 3846.

[5] S. Ida, Y. Sonoda, K. Ikeue, Y. Matsumoto, *Chem. Commun.* **2010**, *46*, 877.

[6] K.-H. Lee, B.-I. Lee, J.-H.You, S.-H. Byeon, *Chem.Commun.* **2010**, *46*, 1461.

[7] Y.-s. Yoon, S.-H. Byeon, I. S. Lee, *Adv. Mater.* **2010**, *22*, 3272.

[8] a) D. Wan, H.-L. Chen, T.-C. Tseng, C.-Y. Fang, Y.-S. Lai, F.-Y. Yeh, *Adv. Funct. Mater.* **2010**, *20*, 3064; b) S. Diedenhofen, G. Vecchi, R. E. Algra, A. Hartsuiker, O. L. Muskens, G. Immink, E. P. A. M. Bakkers, W. L. Vos, J. G. Rivas, *Adv. Mater.* **2009**, *21*, 973; c) M. Kim, K. Kim, N. Y. Lee, K. Shin, Y. S. Kim, *Chem. Commun.* **2007**, *22*, 2237; d) Z. Wu, D. Lee, M. F. Rubner, R. E. Cohen, *Small* **2007**, *3*, 1445.

[9] H. A. Macleod, in *Thin-Film Optical Filters*, Hilger, Bristol **1986**.

[10] a) D. Lee, M. F. Rubner, R. E. Cohen, *Nano Lett.* **2006**, *6*, 2305; b) F. C. Cebeci, Z. Wu, L. Zhai, R. E. Cohen, M. F. Rubner, *Langmuir* **2006**, *22*, 2856; c) J. Park, L. D. Fouche, P. T. Hammond, *Adv. Mater.* **2005**, *17*, 2575; d) J. H. Rouse, G. S. Ferguson, *J. Am. Chem. Soc.* **2003**, *125*, 15529; e) N. Krasteva, I. Besnard, B. Guse, R. E. Bauer, K. Mullen, A. Yasuda, T. Vossmeyer, *Nano Lett.* **2002**, *2*, 551.

[11] a) Moran Wang, A. Revil, *J. Colloid Interface Sci.* **2010**, *343*, 381; b) D. Lee, Z. Gemici, M. F. Rubner, R. E. Cohen, *Langmuir* **2007**, *23*, 8833; c) D. G. Shchukin, M. Zheludkevich, K. Yasakau, S. Lamaka, M. G. S. Ferreira, H. Möhwald, *Adv. Mater.* **2006**, *18*, 1672; d) Y. Lvov, K. Ariga, M. Onda, I. Ichinose, T. Kunitake, *Langmuir* **1997**, *13*, 6195.

[12] R. K. Iler, *J. Colloid Interface Sci.* **1966**, *21*, 569.

[13] X.-T. Zhang, O. Sato, M. Taguchi, Y. Einaga, T. Murakami, A. Fujishima, *Chem. Mater.* **2005**, *17*, 696.

[14] J. C. Park, H. K. Moon, D. K. Kim, S. H. Byeon, B. C. Kim, K. S. Suh, *Appl. Phys. Lett.* **2000**, *77*, 2162.

[15] a) B. Mercier, C. Dujardin, G. Ledoux, C. Louis, O. Tillement, *J. Appl. Phys.* **2004**, *96*, 650; b) W. O. Gordon, J. A. Carter, B. M. Tissue, *J. Lumin.* **2004**, *108*, 339.

[16] B.-I. Lee, K. S. Lee, J. H. Lee, I. S. Lee, S.-H. Byeon, *Dalton Trans.* **2009**, 2490.

[17] F. X. Geng, Y. Matsushita, R. Ma, H. Xin, M. Tanaka, F. Izumi, N. Iyi, T. Sasaki, *J. Am. Chem. Soc.* **2008**, *130*, 16344.

[18] G. Blasse, B. C. Grabmaier, in *Luminescence Materials*, Springer, Berlin, Heidelberg **1994**.

[19] R. C. Ropp, in *Luminescence and the Solid State*, Elsevier, Amsterdam **1991**.

[20] a) Y.-S. Park, J.-W. Kang, D. M. Kang, J.-W. Park, Y.-H. Kim, S.-K. Kwon, J.-J. Kim, *Adv. Mater.* **2008**, *20*, 1957; b) S. R. Amrutha, M. Jayakannan, *J. Phys. Chem. B* **2008**, *112*, 1119.